Gómez-de la Cruz, F. J., Palomar-Carnicero, J. M., Hernández-Escobedo, Q., & Cruz-Peragón, F. (2020). Determination of the drying rate and effective diffusivity coefficients during convective drying of two-phase olive mill waste at rotary dryers drying conditions for their application. *Renewable Energy*, *153*, 900-910.

https://doi.org/10.1016/j.renene.2020.02.062

Determination of the drying rate and effective diffusivity coefficients during convective drying of two-phase olive mill waste at rotary dryers drying conditions for their application.

Authors.

Francisco J. Gómez-de la Cruz[1*], José M. Palomar-Carnicero[1], Quetzalcoatl Hernández-Escobedo[2], Fernando Cruz-Peragón[1].

[1]Dep. of Mechanical and Mining Engineering, Escuela Politécnica Superior de Jaén, University of Jaén, Campus Las Lagunillas s/n, 23071, Jaén (Spain).

[2]Escuela Nacional de Estudios Superiores Juriquilla, UNAM, Queretaro 76230, Mexico.

Abstract.

Secondary extraction factories in the oil olive production are subjected to high pressures each year due to the treatment of large quantities of olive mill wastes. In return, this sector achieves a biomass by-product and olive pomace oil. Furthermore, these facilities remove a serious environmental problem. To help improve and optimize the drying process of these wastes, we have carried out a study of mass transfer in a convective dryer using the drying conditions in rotary dryers. A design of experiments based on a central composite design in two dimensions, drying air temperature (between 100ºC and 425ºC) and drying air velocity (between 1 m/s and 7 m/s), was used to determine the drying rate and effective diffusivity coefficients. These variables were calculated from the experimental data obtained in isothermal drying test. Polynomial surface models, obtained by the linear least-squares fitting method, allowed to calculate these variables as a function of other such as drying air temperature, drying air velocity and moisture ratio. Drying rate and effective diffusivity values were found between

*Corresponding author: Tel.: +34 953213002; Fax: +34 953212870; E-mail address: fjgomez@ujaen.es

0.00001915 and 0.028 $kg_{water}/kg_{solid}\cdot s$ and $1.917\cdot10^{-8}$ and $10.02\cdot10^{-8}$ m^2/s, respectively. These parameters will contribute to solve the heat and mass transfer phenomena in rotary dryers.

Keywords: Drying rate; Effective diffusivity; Olive mill wastes; Modelling; Rotary dryers.

Nomenclature

a, b, c, d, e, f, n	Coefficients of the mathematical models
c_p	Specific heat at constant pressure ($kJ\cdot kg^{-1}\cdot K^{-1}$)
D_{eff}	Effective diffusivity (m^2/s)
D^*_{eff}	Modified effective diffusivity ($m^{0.5}\cdot s^{-0.5}$)
DR	Drying rate ($kg_{water}/(kg_{solid}\cdot s)$)
h_{heat}	Convection heat transfer coefficient ($kW\cdot m^{-2}\cdot K^{-1}$)
h_{mass}	Convection mass transfer coefficient ($m\cdot s^{-1}$)
j	Parameter of fit for modified variable
k	Thermal conductivity ($kW\cdot m^{-1}\cdot K^{-1}$)
K, K_0, K_1	Constants of the mathematical models (s^{-1})
L	Thickness of the slab (m)
Le	Lewis number
λ	Latent heat ($kJ\cdot kg^{-1}$)
$\dot{m}$	Mass flow ($kg\cdot s^{-1}$)
R^2	Coefficient of determination
$RMSE$	Root mean square error

S	Slope of the linear approach (s^{-1})
t	Time (s)
T	Temperature (ºC, K)
T^*	Temperature ratio
U	Volumetric heat transfer coefficient ($kW \cdot m^{-3} \cdot K^{-1}$)
v	Velocity ($m \cdot s^{-1}$)
V	Volume (m^3)
x	Spatial dimension (m)
X_e	Equilibrium moisture content (kg moisture/kg dry matter)
X_0	Initial moisture content (kg moisture/kg dry matter)
X_t	Moisture content at time t (kg moisture/kg dry matter)
XR	Dimensionless moisture ratio
x_v	Drying rate (s^{-1})
x_v^*	Modified drying rate ($m^{0.5} \cdot s^{-0.5}$)

Subindex

a	Air
cal	Calculated
da	Dry air
dp	Dry product
exp	Experimental
min	Minimum
max	Maximum
p	Product

w	Water
v	Vapor
$surf$	Surface

1. Introduction.

Olive oil production represents the 1,7 % share of total output of edible vegetable and animal fats. It is one of the most important ingredients in the Mediterranean diet due to its antioxidant properties to prevent diseases like cancer, cardiovascular problems, diabetes and obesity, among others. In the last olive crop year, 2018/2019, olive oil world production was 3,100,000 tonnes [1]. Spain is the world's top producer and exporter of olive oil whose production represents 50% of total output [2]. Sixty per cent of the total olive acreage is located in Andalusia, the southern region of Spain, which produces 1,350,000 tonnes (85% of the Spain's production, and 43% of the world's production).

During the olive oil extraction process, large quantities of olive mill wastes are generated [3]. Only in Spain, more than 6,000,000 tonnes of olive mill wastes, mainly two-phase olive mill wastes, were treated in their sixty-three secondary extraction factories. These facilities play the role most important in the olive oil life cycle since if the olive mill wastes treatment stopped, the olive oil production would stop as well [4]. Therefore, the foremost aim of these factories is to remove a serious environmental problem [5]. In return, secondary extraction factories obtain three by-products which provide them with benefits: crude olive pomace oil, dry de-oiled pomace and olive stone [6,7]. Nowadays, this sector has serious profitability problems because of the low prices of their principal by-products. Crude olive pomace oil is extracted by solvents

when drying of these wastes reaches the equilibrium moisture content (8%, wet basis), and then is refined and blended with olive virgin oils to obtain the olive pomace oil [8]. Dry de-oiled pomace, which is exported to the European Union countries, is used as biomass with a net calorific value of 17.5 MJ/kg in industrial boilers for the electrical and thermal energy production [9,10]. And the olive stone (fragments of endocarp), with a net calorific value of 19.2 MJ/kg, is destined as biomass in heating boilers for thermal purposes in the industry and for space heating in commercial building and homes [11-15]. However, its main challenge is to receive and treat large quantities of these wastes in short periods due to uninterrupted harvesting seasons.

The principal method to eliminate olive mill wastes is drying in industrial concurrent rotary dryers [16,17]. Mainly, two-phase olive mill wastes, with an initial moisture content between 60% and 75% (wet basis), is dried at high inlet drying air temperatures (400ºC-800ºC) and drying air velocities (1-7 m/s). Hot drying gases are obtained from the combustion of the dry de-oiled pomace in furnaces or using cogeneration systems from reciprocating internal combustion engines [18]. This waste is a thick sludge formed by vegetable water, olive stones, pulp, skin, sugars and olive oil (about 3%).

Drying of olive mill wastes has been widely researched and debated in the literature. Celma et al. (2007), Montero (2010) et al., Montero et al. (2011) and Montero et al (2015) have studied the drying kinetics of the three and two-phase olive mill wastes in solar dryers of different kinds like passive, active and hybrid. Drying was carried out at temperatures between 20ºC and 80ºC, at different drying air velocities, up to 7 m/s, and at different sample thicknesses, between 6.2 mm and 40 mm [19-22]. Liébanes et al. (2006) and Meziane (2011) carried out experiments in a fluidized bed dryer about drying of two-phase olive mill wastes and three-phase olive mill wastes,

126 respectively [23,24]. They worked using drying air temperatures between 50ºC and
127 130ºC, drying air velocities between 1 m/s and 2.5 m/s and sample thicknesses between
128 41 mm and 63 mm. Arjona et al. (1999), Krokida et al. (2002), Vega-Gálvez et al.
129 (2010), Casanova-Peláez et al. (2015) using convective dryers for drying of two-phase
130 olive mill wastes [25-28]. And Doymaz et al. (2004), Akgun and Doymaz (2005) and
131 Gogus and Maskan (2006) did the same with three-phase olive mill wastes [29,30]. In
132 these experiments, the range of parameters tested was from 50ºC to 350ºC for
133 temperature, from 1.2 m/s to 3 m/s for air velocity and from 4 mm to 72 mm for sample
134 thickness. Milczarek et al. (2011) used a microwaves-convective dryer for drying of
135 two-phase olive mill wastes at low temperatures, between 40ºC and 70ºC, and a drying
136 air velocity and sample thickness of 4 m/s and 7 mm, respectively [31]. Gögus and
137 Maskan (2001) worked with the same type of dryer to dry three-phase olive mill wastes
138 at temperatures up to 225ºC and different sample thicknesses, between 6 mm and 14
139 mm [32]. Finally, Ruiz Celma et al. (2008) studied drying of the three phase-olive oil
140 mill wastes in an infrared dryer at temperatures between 80ºC and 140ºC for a sample
141 thickness of 7 mm [33].
142 However, these researches carried out in all these types of dryers have not industrial
143 applications in nowadays. As mentioned above, practically all drying of olive mill
144 wastes is dried in industrial concurrent rotary dryers. These dryers allow to dry between
145 10,000 kg/h and 15,000 kg/h of these wastes, which continue to be the sole equipment
146 that are able to treat them in a few months. However, because of its heterogeneity and
147 high moisture content, the drying process is a complex phenomenon, making it
148 extremely difficult to study by physical models [34]. Thus, it is necessary to address this
149 problem carrying out a parametric study of the main variables involved in the process.
150 Variables like drying air temperature, drying air velocity, moisture content, drying rate

151 and effective diffusivity coefficients are essential to study the drying process in rotary
152 dryers from the sectioned models [35]. These models study the laws of conservation of
153 mass and energy in the trommel from discretized models dividing the trommel length in
154 sections.

155 In this paper, we performed the drying of two-phase olive mill waste in a
156 convective dryer from an experimental design based on nine isothermal tests using the
157 drying conditions in industrial rotary dryers (high drying air temperatures and
158 velocities). The main goal is to calculate, the drying times, the drying rates and effective
159 diffusivity coefficients taking into account the real drying conditions in order to be
160 applied in future works using sectioned models in rotary dryers. In this sense, future
161 improvements will be explicitly linked to the modeling, control, optimization and
162 automation of the drying process [36].

163

164 ## 2. **Materials and methods.**

165

166 ### 2.1. Raw material.

167

168 Two-phase olive mill waste samples were kindly provided by several secondary
169 extraction factories and olive oil mills in the province of Jaén (Spain). Samples were
170 studied as received. Initial moisture content was obtained from drying of the samples in
171 an oven (Memmert GmbH+Co.KG, SNB 167 Model 100, Germany) at 105ºC during 24
172 hours in triplicate. The average initial moisture content value was established in 61 ±
173 0.5 % (wet basis). On the other hand, equilibrium moisture content was found out using
174 the same procedure to obtain a value of 8.5 ± 0.2% (wet basis). The room temperature
175 was 20ºC and the relative humidity of the air 50 %. The final analysis revealed the

following composition: moisture content (61%), olive stones (6.5%), oil content (2.4 %), pulp, skin and other components (30.1%).

On the other hand, an ultimate analysis of two-phase olive mill waste was obtained using a LECO TruSpec CHN2 elemental analyzer according to ASTM D5373. A proximate analysis was carried out by a Thermogravimetric Analyzer TGA (Mettler Toledo) as well. Furthermore, the higher heating value (HHV) and net calorific value (NCV) of this waste were determined using the PARR 6050 bomb calorimeter according to ASTM D240 standard. All these analysis were performed in triplicate. Table 1 exhibits the results obtained.

Table 1. Ultimate analysis, proximate analysis and higher heating value (HHV) and net calorific value (NCV) of two-phase olive mill waste.

Analysis	Element	Value
Elemental analysis (%)	C	51.06
	H	6.14
	N	0.89
	S	0.08
	O (by difference)	27.52
Proximate analysis (%)	Moisture	0
	Ash	14.31
	Volatile Matter	67.16
	Fixed Carbon (by difference)	18.53
Higher Heating Value (HHV) (MJ/kg)		19.76
Net Calorfic Value (NCV) (MJ/kg)		18.48

2.2. Drying equipment.

The experimental equipment consists mainly of a blower, a group of electrical resistances and an insulated drying channel that transports the hot air toward the samples (figure 1).

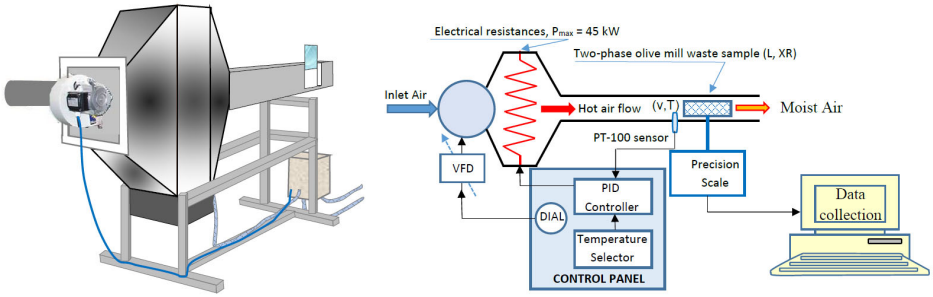

Figure 1. Experimental drying equipment.

- The blower of medium pressure and simple aspiration presents a maximum value of air flow of 475 m^3/h at 2900 rpm with a power of 80 W. Air flow is regulated by variable frequency drive connected to an electric AC motor. Air velocity is measured from a pitot tube and TESTO manometer in the PVC tube joined to the blower.
- Electrical resistances, T-MAX-45 ELECTRICFOR model, are composed by 30 units divided in three stages: two resistors of 18 kW and one resistor of 9 kW, in total 45 kW. Air flow passing through the electrical resistances to be heated at the operating temperature. Drying temperature is controlled by a PT100 sensor connected with a proportional-integral-derivative control (PID), which acts on the electrical resistances. The sensor is placed just before the basket.
- Hot air is directed by the insulated drying channel to the sample, which is located at the end. Dimensions of the channel are 2 m of length with a square section of 15 cm x 15 cm. Two-phase olive mill waste samples were deposited on the rectangular basket with average dimensions of a flight in rotary dryers, 100 mm of width and 250 mm of length. The basket was placed over a precision scale (BLAUSCAL AH1200) with an

217 approximation error of $\pm 0.01 \cdot 10^3$ kg, which was connected to a personal
218 computer by USB port. A software programmed by us collects and saves the
219 experimental data (variation of mass) in MATLAB® files.
220 When the steady-state conditions for each test were reached, samples were entered
221 into the channel. Tests stopped when the equilibrium moisture content was
222 approximately achieved or when samples began to burn. To find out the final moisture
223 content, samples were dried in the oven during 24 hours at 105ºC.
224
225 2.3. Experimental setup.
226
227 Taking into account the drying real conditions in rotary dryers, especially facilities
228 that use hot gases drawn principally from gas turbines or reciprocating internal
229 combustion engines, a central composite design in two dimensions, drying air
230 temperature and drying air velocity, was proposed. This design of experiments allow
231 covering a wide range of the drying conditions in rotary dryers of two-phase olive mill
232 waste without the need to raise the number of experiments. Drying temperature ranges
233 between 100 ºC and 425ºC and drying air velocity ranges between 1 m/s and 7 m/s. All
234 experiments used a sample thickness of 20 mm, which simulated the material thickness
235 that is rotate at every turn by the flights of the rotary dryer. Figure 2 shows the chosen
236 experimental plan, nine isothermal experiments in total.
237

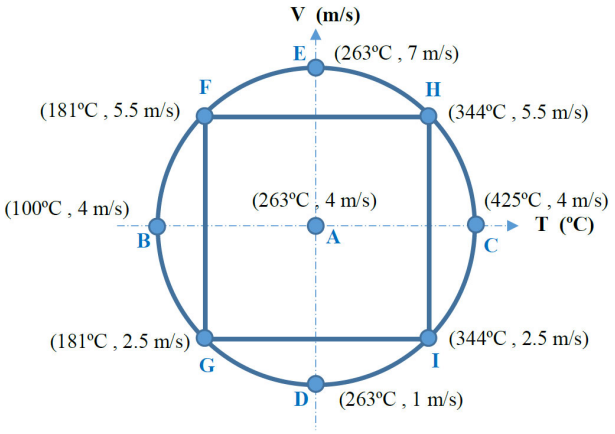

Figure 2. Design of experiments based on central composite design in two dimension.

2.4. Mathematical models of drying curves, drying rate and effective diffusivity.

Drying is a complex physic phenomenon based on simultaneous coupled heat and mass transfer that includes several manifestations in the water elimination process. For this reason, frequently researchers use mathematical models that fit faithfully drying curves or drying times.

Drying curves analyze the variation of moisture content with respect to time, $XR = f(t)$. The moisture ratio can be written as:

$$XR = \frac{X_t - X_{eq}}{X_0 - X_{eq}} \quad (1)$$

Where X_t is the moisture content at time t, X_0 is the initial moisture content, and X_{eq} is the equilibrium moisture content, all these values expressed in dry basis (kg_{water}/kg_{solid}). However, moisture ratio can be obtained using the relation X_t/X_0 due to X_{eq} is very small with regard to X_0.

In this study, we have carried out the approximation of drying curves from the main

mathematical models proposed in the literature for each experiment (table 2) [11]. The quality of fit in these models is calculated from statistical tests using the coefficient of determination (R^2) and the root mean square error ($RMSE$):

$$R^2 = \sum_{i=1}^{N} \frac{\left(XR_{cal,i} - XR_{exp,i}\right)^2}{\left(XR_{exp,i} - \overline{XR_{exp,i}}\right)^2} \quad (2)$$

$$RMSE = \sqrt{\frac{1}{N}\sum_{I=1}^{N}\left(XR_{exp,i} - XR_{cal,i}\right)^2} \quad (3)$$

Where N is the number of data and the subscripts exp and cal mean experimental and calculated, respectively.

Table 2. Mathematical models proposed to study the drying curves of the two-phase olive mill waste.

Model name	Equation	Authors
Approach of diffusion	$XR = a \cdot \exp(-kt) + (1-a) \cdot \exp(-kbt)$	Yaldiz et al., 2001
Henderson and Pabis	$XR = a \cdot \exp(-kt)$	Henderson and Pabis, 1961
Midilli et al.	$XR = a \cdot \exp(-kt^n) + bt$	Midilli et al., 2002
Page	$XR = \exp(-kt^n)$	Page, 1949
Two term	$XR = a \cdot \exp(-k_0 t) + c \cdot \exp(-k_1 t)$	Noomhorm and Verma, 1986
Two term Gaussian	$XR = a \cdot \exp\left[-\left(\frac{t-b}{c}\right)^2\right] + d \cdot \exp\left[-\left(\frac{t-e}{f}\right)^2\right]$	Gómez-de la Cruz et al., 2014
Wang and Singh	$XR = 1 + at + bt^2$	Wang and Singh, 1978

Mathematical models provide the drying times for each test. Drying rates can be calculated from the derivate of these functions, which fits the drying curves [11]. Drying rate is a variable that explain the variation of moisture content with regard to time, in other words, the velocity of water elimination in the solid. This value can be written as:

$$x_v = -\frac{dXR}{dt} \approx -\frac{XR_{t+\Delta t} - XR_t}{\Delta t} \quad (4)$$

where $XR_{t+\Delta t}$ and XR_t represent the moisture content at time $t + \Delta t$ and the moisture content at time t, respectively, and t is the drying time. Here, the minus sign is a consequence of the fact that moisture ratio decreases when the drying time increases.

This variable is very important during the drying process in rotary dryers, since it will allow to calculate the water elimination for each section of the trommel knowing the main parameters that affect the drying process. In fact, drying rate can be expressed as a function of the moisture content of the sample at any time, since the moisture content depends on the drying time, $x_v = f(XR)$. Drying rate in $kg_{water}/kg_{solid} \cdot s$, DR, is calculated multiplying x_v by X_0. Finally, the design of experiments allows to obtain the drying rate as a general function that depends on the drying air velocity, drying air temperature and moisture ratio, $x_v = f(T, XR, v)$. For that, a new variable, modified drying rate, is obtained as follows:

$$x_v^* = \frac{x_v \cdot L}{v^j} \quad (5)$$

This association of parameters (a pseudo-dimensionless number) can be expressed as a function of moisture ratio and temperature ratio, $x_v^* = f(T^*, XR)$, and j is a parameter that fits the drying rate curves for the test carried out at the same temperature. The temperature ratio can be expressed as:

$$T^* = \frac{T - T_{min}}{T_{max} - T_{min}} \quad (6)$$

In this equation, T is the value of temperature in the drying process, and T_{min} and T_{max} are the minimum and maximum values of the design of experiments, respectively.

303 Therefore, drying rate can be obtained in all situations of the drying process as follows:

304

305 $$x_v = \frac{x_v^*(T^*,XR)\cdot v^j}{L} \quad (7)$$

306

307 Another important variable in the drying process is the effective diffusivity. In this
308 study, effective diffusivity is an experimental global parameter that includes all physic
309 phenomena that affect in the drying process. In this sense, these values are utilized to
310 measure the variation of moisture content regardless of the phenomena that occur
311 [13,37].

312 Moisture transport mechanisms are usually explain from the Fick' second law
313 diffusion as follows:

314

315 $$\frac{\partial XR}{\partial t} = D_{eff}\nabla^2 XR \quad (8)$$

316

317 In this equation, D_{eff} is the effective diffusivity (m^2/s), XR is the moisture ratio and t is
318 the time (s). The solution for slab geometry proposed in this study and considering
319 transport only in the x axis was obtained by Crank (1975) as follows [38]:

320

321 $$XR = \frac{8}{\pi^2}\sum_{n=0}^{\infty}(x(n))^{-2}e^{-\frac{(x(n))^2\pi^2 D_{eff}}{L^2}t} \quad (9)$$

322

323 where L is the sample thickness (m) and the $x(n)$ is expressed as $2n+1$. The solution
324 is particularized to the first term undertaking errors very small when time is very long.
325 The solution can be rewritten as:

326

$$XR = \frac{8}{\pi^2} e^{-\frac{\pi^2 D_{eff}}{L^2} t} \quad (10)$$

Effective diffusivity values can be calculated from experimental data of drying experiments representing the $\ln(XR)$ with regard to time using the simplified method as follows [13]:

$$D_{eff} = -S \cdot \frac{L^2}{\pi^2} \quad (11)$$

where S is the slope of the linear function which fits $\ln XR$ vs. time. Statistical criteria from eqs. (2) and (3) were used to find out the quality of fit. On the other hand, experimental data, $\ln XR$ vs. time, does not present a good fit with linear approximation. In this sense, the simplified modified method, which uses polynomial models to fit data, allows to obtain values of the time-dependent effective diffusivity and, therefore, as a function of moisture ratio [13]. These values are obtained from modified eq. (8) as follows:

$$D_{eff}(t) = -\frac{d(\ln XR)}{dt} \cdot \frac{L^2}{\pi^2} \quad (12)$$

Thus, constant values of this variable are replaced by functions that depend on the moisture ratio ($D_{eff} = f(XR)$) which makes future calculations are more accurate. Furthermore, just as for the drying rate, a general expression can be obtained from the drying air temperature, moisture ratio and drying air velocity, $D_{eff} = f(T, XR, v)$, using an association of parameters for effective diffusivity as follows:

$$D^*_{eff} = \frac{D_{eff}}{L \cdot v^j} \quad (13)$$

Newly, modified effective diffusivity can be expressed with respect to moisture ratio and temperature ratio, $D^*_{eff} = f(XR, T^*)$. And effective diffusivity can be written as:

$$D_{eff} = D^*_{eff}(XR, T^*) \cdot L \cdot v^j \quad (14)$$

2.5. Description of the methodology for futures applications in rotary dryers.

One of the main problems in the study of heat and mass transfer models in rotary dryers is to know the drying rate values along to the trommel length. With the sectioned trommel model, rotary dryers can be studied dividing the trommel in small control volumes [35]. Mass and energy conservation equations for this model are proposed as follows:

$$\frac{\partial (m_{da})^{(i)}}{\partial t} = \dot{m}_{da}{}^{(i-1)} - \dot{m}_{da}{}^{(i)} \quad (15)$$

$$\frac{\partial (m_{dp})^{(i)}}{\partial t} = \dot{m}_{dp}{}^{(i-1)} - \dot{m}_{dp}{}^{(i)} \quad (16)$$

$$\frac{\partial (m_{w})^{(i)}}{\partial t} = \dot{m}_{w,p}{}^{(i-1)} - \dot{m}_{w,p}{}^{(i)} - DR \cdot m_{dp}{}^{(i)} \quad (17)$$

$$\frac{\partial (m_{v})^{(i)}}{\partial t} = \dot{m}_{v}{}^{(i-1)} - \dot{m}_{v}{}^{(i)} + DR \cdot m_{dp}{}^{(i)} \quad (18)$$

$$\frac{\partial\left(m_{dp}^{(i)}\cdot c_{p,dp}^{(i)}+m_{w}^{(i)}\cdot c_{p,w}^{(i)}\right)T_{p}^{(i)}}{\partial t}=U^{(i)}V\left(T_{a}^{(i)}-T_{p}^{(i)}\right)+\left(\dot{m}_{dp}^{(i)}\cdot c_{p,dp}^{(i)}+\dot{m}_{w}^{(i)}\cdot c_{p,w}^{(i)}\right)T_{p}^{(i)}-\left(\dot{m}_{dp}^{(i-1)}\cdot c_{p,dp}^{(i-1)}+\dot{m}_{w}^{(i-1)}\cdot c_{p,w}^{(i-1)}\right)T_{p}^{(i-1)}-DR\cdot m_{dp}{}^{(i)}(c_{p,w}^{(i)}\cdot T_{p}^{(i)}+\lambda) \quad (19)$$

$$\frac{\partial\left(m_{v}^{(i)}\cdot c_{p,v}^{(i)}+m_{da}^{(i)}\cdot c_{p,da}^{(i)}\right)T_{a}^{(i)}}{\partial t}=-U^{(i)}V\left(T_{a}^{(i)}-T_{p}^{(i)}\right)+\left(\dot{m}_{da}^{(i)}\cdot c_{p,da}^{(i)}+\dot{m}_{v}^{(i)}\cdot c_{p,v}^{(i)}\right)T_{a}^{(i)}-\left(\dot{m}_{da}^{(i-1)}\cdot c_{p,da}^{(i-1)}+\dot{m}_{v}^{(i-1)}\cdot c_{p,v}^{(i-1)}\right)T_{a}^{(i-1)}+DR\cdot m_{dp}{}^{(i)}\cdot c_{p,v}^{(i)}(T_{a}^{(i)}-T_{p}^{(i)}) \quad (20)$$

Eqs. (15-18) analyze the mass transfer between sections in dry air, dry by-product, water and vapor, respectively. Eqs. (19-20) analyze the heat transfer between sections in the by-product and the drying air. In these equations, m is the mass, c_p is the specific heat at constant pressure, U is the volumetric heat transfer coefficient, V is the volume, λ is the latent heat and T is the temperature. Superscripts (i) and (i-1) represent the studied section and the previous section respectively.

In all these equations, drying rate appears as an unknown variable. In fact, in nowadays drying rate only can be obtained as an average value between the inlet and outlet of the rotary dryers. In this sense, drying rate values obtained in this study can be used in each section of the rotary dryer when the by-product is raised by the flights, no matter what happens between sections. Knowing the drying air temperature, drying air velocity and the moisture content in each section of the trommel, the drying rate is defined, $DR = f(T, XR, v, X_0)$ [36].

On the other hand, effective diffusivity coefficients allow studying the heat and mass transfer near to the sample (inside and boundary), which is turned by the flights. First, effective diffusivity studies the mass transport in the sample using the Fick's law of diffusion. Nevertheless, in rotary dryers, it is more important to analyze this problem in the boundary of the sample. Therefore, parameters like convection mass transfer

coefficient and convection heat transfer coefficient can be obtained as follows:

$$h_{mass} = \frac{-D_{eff} \cdot \frac{\partial X}{\partial x}\Big|_{x=L}}{X_{surf} - X_a} \quad (21)$$

$$h_{heat} = h_{mass} \frac{k}{D_{eff} \cdot Le^n} \quad (22)$$

Convection heat transfer coefficient is calculated using the analogy between concentration and thermal boundary layers; where k is the thermal conductivity, Le is the Lewis number and n is a constant that generally assumes a value of 0.33 for most applications. Furthermore, drying rate can be used for verifications in the boundary of the samples as follows:

$$-D_{eff} \cdot \frac{\partial X}{\partial x}\Big|_{x=L} = DR \cdot L \quad (23)$$

All these parameters will be used to obtain a mathematical model from neural networks or auto-regression with exogenous variables (ARXs). Subsequently CFD techniques will be utilized with the objective of helping to solve the heat and mass transfer of two-phase olive mill waste in rotary dyers. Figure 3 shows a scheme of the methodology proposed and the drying process in rotary dryers.

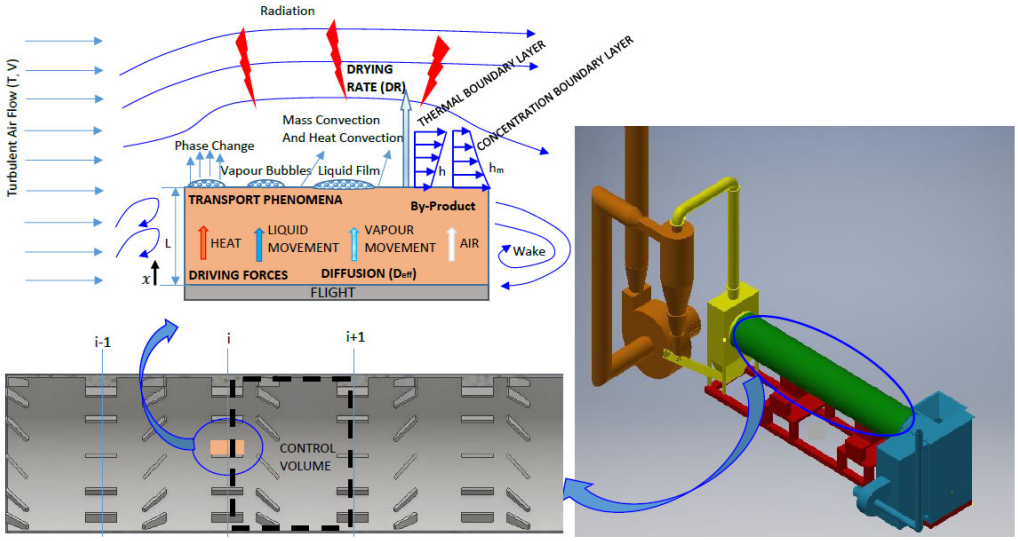

Figure 3. Methodological scheme of the drying process in two-phase olive mill waste rotary dryers.

3. Results and discussion.

3.1 Analysis of the drying time and drying rate from isothermal drying experiments.

Moisture ratio was plotted using the time as independent variable for each of the nine experiments (Figure 4). Results reveal that short drying time is linked to high drying temperatures and high air velocities. Likewise, all test carried out at temperatures above 200ºC: tests A, C, D, E, H and I experimented the combustion phenomenon. Combustion was reached in tests A, D, E and I when the moisture content was close to equilibrium moisture content. However, in the tests C and H, samples started to burn at moisture content of 23% and 30%, respectively. This fact evidenced the risk of fire in rotary dryer during the drying of two-phase olive mill waste. However, high drying temperatures are manifested in the first sections of the trommel where the moisture content is high and, on the other hand, the equilibrium moisture content is reached at the

end of the trommel where the drying air temperature ranges between 90ºC and 110ºC. Furthermore, in all experiments performed at temperatures above 200ºC, appeared the release of volatile matter just before the start of combustion. During the experiments, no considerable shrinkage in the samples was appreciated.

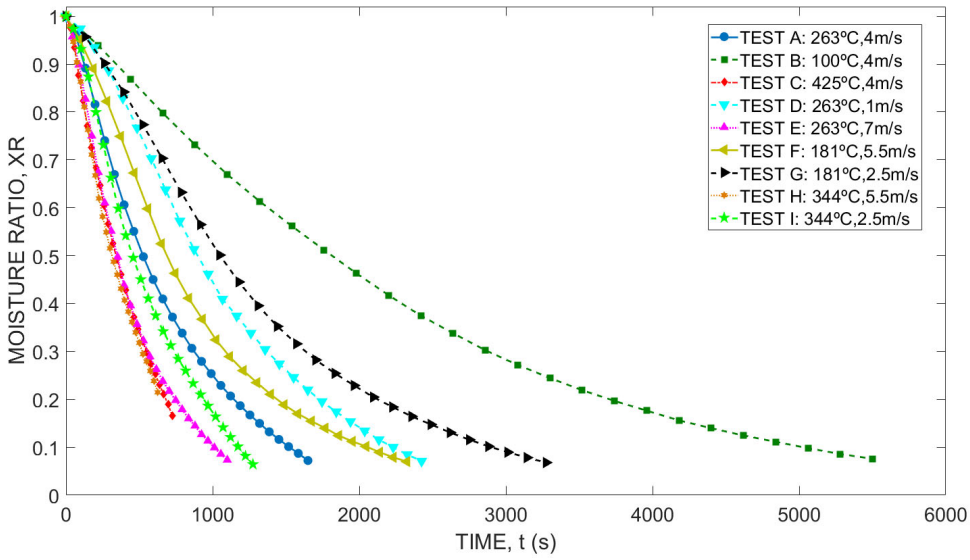

Figure 4. Drying curves for each experiments carried out in the convective dryer.

Drying curves were fitted with the mathematical models of the table 2. Results of quality of fit for each model are indicated in table 3.

Table 3. Goodness of fit with 95 % confidence bounds in the main mathematical models to approach drying curves.

	Approach of Diffusion		Henderson and Pabis		Midilli et al.		Page		Two-Term		Two-Term Gaussian		Wang and Singh	
	R^2	RMSE	R^2	RMSE	R^2	RMSE	R^2	RMSE	R^2	RMSE	R^2	RMSE	R^2	RMSE
TEST A	0.9969	0.0168	0.9969	0.0164	0.9993	0.0080	0.9984	0.0118	0.9987	0.0113	0.9999	0.0037	0.9971	0.0159
TEST B	0.9986	0.0111	0.9961	0.0183	0.9999	0.0022	0.9999	0.0028	0.9999	0.0022	0.9999	0.0034	0.9995	0.0069
TEST C	0.9980	0.0121	0.9945	0.0197	0.9996	0.0055	0.9994	0.0064	0.9938	0.0218	0.9998	0.0036	0.9985	0.0102
TEST D	0.9997	0.0060	0.9832	0.0408	0.9990	0.0103	0.9974	0.0156	0.9997	0.0061	0.9977	0.0167	0.9915	0.0289
TEST E	0.9946	0.0224	0.9956	0.0197	0.9994	0.0079	0.9986	0.0110	0.9998	0.0046	0.9999	0.0031	0.9965	0.0176
TEST F	0.9994	0.0073	0.9940	0.0235	0.9988	0.0106	0.9976	0.0146	0.9956	0.0210	1.0000	0.0014	0.9956	0.0203
TEST G	0.9997	0.0050	0.9914	0.0286	0.9987	0.0117	0.9987	0.0111	0.9998	0.0050	0.9974	0.0171	0.9955	0.0206
TEST H	0.9944	0.0195	0.9952	0.0176	0.9987	0.0095	0.9980	0.0112	0.9996	0.0056	0.9999	0.0021	0.9953	0.0175
TEST I	0.9933	0.0254	0.9898	0.0307	0.9983	0.0129	0.9980	0.0134	0.9968	0.0180	0.9999	0.0026	0.9948	0.0220
AVERAGE	0.9972	0.0139	0.9929	0.02392	0.9991	0.0087	0.9984	0.0109	0.9982	0.0106	0.9994	0.0059	0.9960	0.0177

Average R^2 and RMSE values reveal that the Two-Term Gaussian model is the best

equation to fit faithfully the experimental data. A good approximation from semi-theoretical and empirical mathematical models is crucial for representing the drying rate curves using the derivate of these models. In fact, small errors in the approximation of drying curves can mean notable errors when the derivate functions is applied. Figure 5 represents the drying rate curves, $x_v = f(XR)$, for each of the experiments, as well as the function that fits the experimental data from the derivate of the Two-Term Gaussian model.

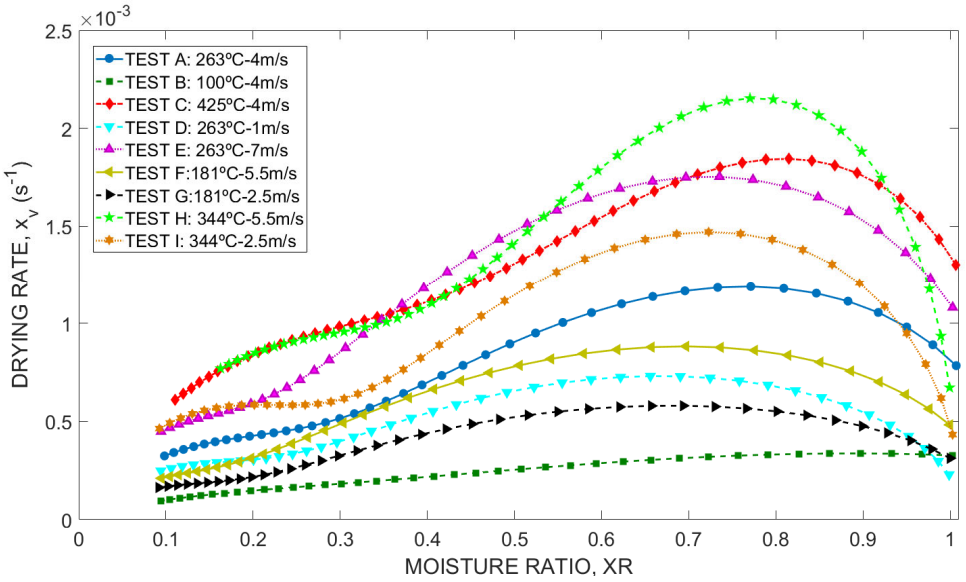

Figure 5. Drying rate curves for each experiments and their fit using the Two-term Gaussian model.

Results evidence newly that higher drying rates are linked at high drying air temperatures and velocities. Although, the mean guiding force in the drying process is the temperature, the air velocity plays a very important role as well. This can be seen in the experiments carried out at 5.5 m/s (TEST H, 344ºC) and 7 m/s (TEST E, 263ºC). Results obtained show that these values are higher than those obtained by different authors throughout literature due to the real drying conditions in rotary dryers [39].

On the other hand, the drying rate variation allows to see the different stages for which proceed the drying process. The warming-up period is manifested at the

beginning of the drying process with a rising drying rate up to a maximum value. Subsequently, a stage characterized by descending drying rate appears until the equilibrium moisture content or the combustion of the sample is reached. This stage is called the falling rate period, which can be divided into two sub stages, the first and second falling rate period. The difference between these two stages can be seen when the slope of the function changes to be less pronounced. The drying process stages have been commented in the literature. Several studies on olive mill wastes present this behavior [11,25,31,40-42].

To obtain the drying rate as a function of moisture ratio, drying air temperature and drying air velocity, the modified drying rate (x_v^*) was fitted using the experimental data of all experiments from a polynomial surface with a fourth degree in T^* and fifth degree in XR (figure 6). To perform the function, the linear least-squares fitting method was used with a coefficient of determination of 0.9802 and a root mean square error of $7.093 \cdot 10^{-7}$. The j parameter was found to be equal to 0.5.

This function will allow for obtaining the drying rate for any condition during the drying process.

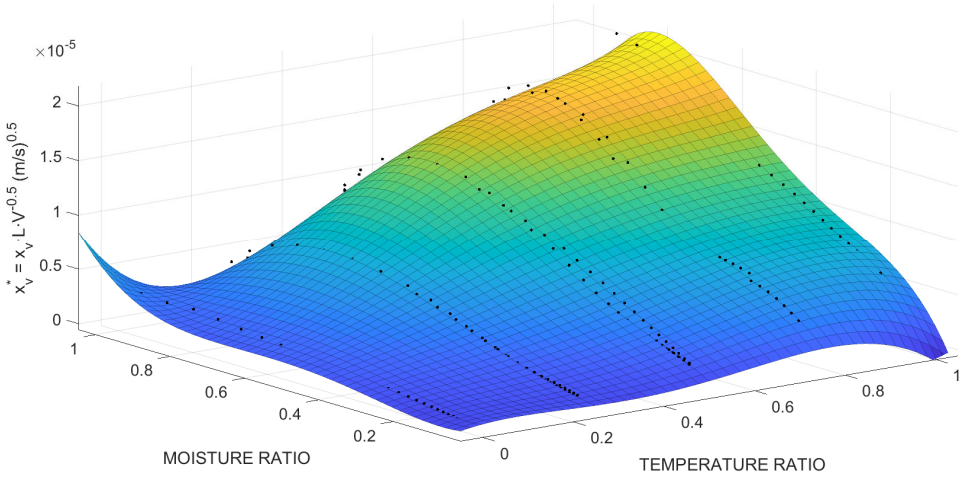

Figure 6. Mathematical function of modified drying rate as a function of moisture ratio and temperature ratio.

3.2 Analysis of the effective diffusivity from isothermal drying experiments.

First, effective diffusivity was calculated to be a constant value for each of the experiments carried out. Table 4 indicates the values of this variable together with the parameters that measure the quality of fit. Figure 7 depicts the tendency of these values taking into account the drying air temperature and velocity.

Table 4. Effective diffusivity values and parameters to verify the quality of fit for each experiment.

	Constant effective diffusivity, D_{eff} (m^2/s) x 10^8	R^2	RMSE
TEST A	6.20	0.9949	0.0576
TEST B	1.917	0.9963	0.0498
TEST C	9.85	0.9926	0.0475
TEST D	4.45	0.9872	0.0946
TEST E	9.59	0.9373	0.0426
TEST F	4.77	0.9986	0.0317
TEST G	3.40	0.9967	0.0496
TEST H	10.02	0.9970	0.0263
TEST I	8.28	0.9802	0.1156

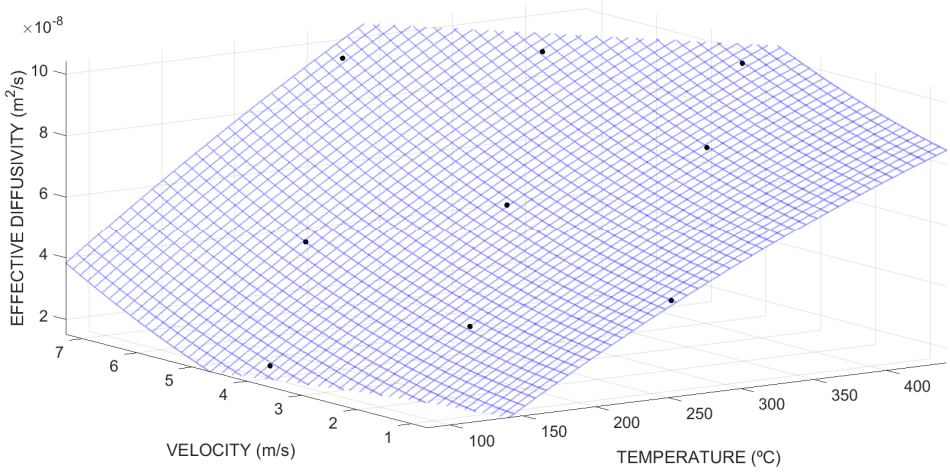

Figure 7. Constant effective diffusivity tendency considering the drying air temperature and velocity.

Results indicate that the values obtained are higher than those found in the literature [39] due to drying conditions in rotary dryers. Just as the drying rate, effective

diffusivity depends heavily on the drying air velocity and drying air temperature.

On the other hand, time-dependent effective diffusivity was calculated as a function of the moisture ratio. For that, experimental data $\ln(XR) - t$, were fitted from a fourth degree polynomial model obtaining an excellent quality of fit, coefficient of determination higher than 0.9999 and a root mean square error lower than 0.008. Figure 8 shows the effective diffusivity when the moisture ratio changes.

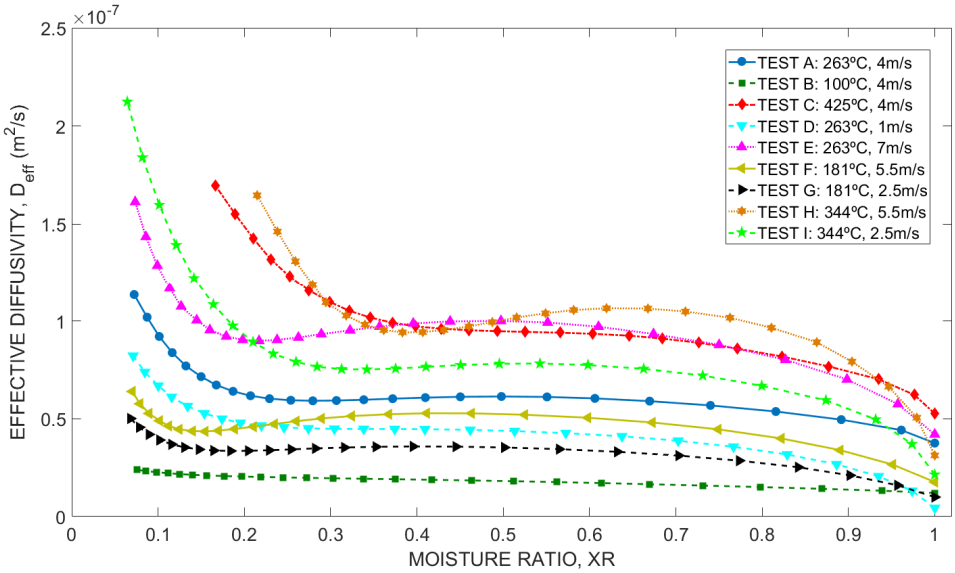

Figure 8. Moisture ratio-dependence effective diffusivity for each test.

The behavior and tendency of these nonlinear logarithmic drying curves have been already seen in other research such as during drying of chitosan [43], during baking of white cake [44] and during drying of olive stone [13]. The evolution of effective diffusivity with respect to moisture ratio can explain, as well as the drying rate, the drying stages: warming up period (between $XR = 1$ and $XR = 0.8$), first falling rate period (between $XR = 0.8$ and $XR = 0.3$) and second falling rate period (for $XR < 0.3$). For high temperature and velocities (higher than 200ºC and velocities equals or higher than 4 m/s), the second falling rate period is characterized by high effective

diffusivity values for low moisture ratios. This can be explained by the fact that for moisture content close to equilibrium moisture content or even, when the surface of the sample is totally dry, the release of volatile matter is notably appreciated.

To complete the study of this variable and to obtain a general function for any drying situation, $D_{eff} = f(T, XR, v)$, modified effective diffusivity was used to found a mathematical function with respect to moisture ratio and temperature ratio. Newly, j parameter was found to be equal to 0.5. Figure 9 exhibits a polynomial surface with a fourth degree in T^* and fifth degree in XR.

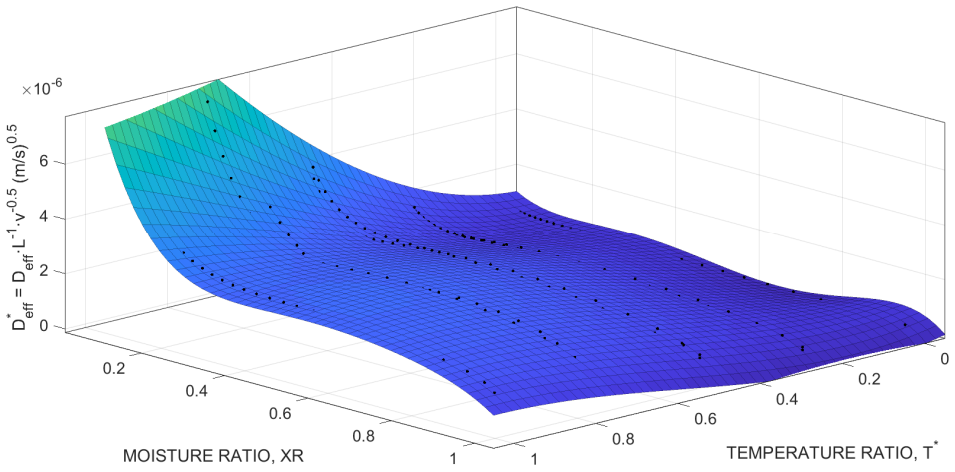

Figure 9. Mathematical function of modified effective diffusivity considering the drying air temperature and velocity.

The linear least-squares fitting method was used again to approach the experimental data obtaining a coefficient of determination of 0.9799 and a root mean square error of $1.591 \cdot 10^{-7}$. Values of effective diffusivity can be calculated from eq. (14) knowing, the temperature and velocity of the drying air and the moisture ratio.

4. Conclusion.

Mass transfer of two-phase olive mill waste during convective drying was analyzed using the drying real conditions in industrial rotary dryers, high drying air temperatures and velocities. Drying rate and effective diffusivity were calculated from the experimental drying curves. Two-term Gaussian model represented faithfully the drying rate for each experiment. Test carried out at temperatures slightly above 200ºC experimented combustion at low moisture content. Samples dried at high temperatures (344ºC and 425ºC) experimented combustion at moisture content between 20 % and 30 % (wet basis). Results showed that higher drying rates and effective diffusivities were linked to high drying temperatures and velocities. The design of experiments allowed to obtain mathematical functions of the drying rate and effective diffusivity whose independent variables are drying air temperature, drying air velocity and moisture ratio, $x_v = f(T, XR, v)$ and $D_{eff} = f(T, XR, v)$, respectively. Using these parameters, other important variables as the convection heat transfer coefficient and the convection mass transfer coefficient can be obtained. All these variables will be used to help solve the complex drying process in industrial rotary dryers taking into account the methodology proposed in section 2.5.

Acknowledgments.

This work has been conducted with the financial support of the Spanish *"Consejería Andaluza de Innovación, Ciencia y Empresa"* through the research project AGR-6131 (*"Modelado y Control de secadero rotativo de orujo"*) as part of the research program *"Proyectos de Excelencia de la Junta de Andalucía 2010-2014"*. The authors gratefully acknowledge the financial support provided. The authors gratefully acknowledge to the association of secondary extraction factories "ANEO*"* the

565 contribution of the two-phase olive mill waste as well.

566

567 **References.**

568

569 [1] International Olive Council (IOC). World olive oil figures: production.
570 Available at: http://www.internationaloliveoil.org/estaticos/view/131-world-olive-oil-
571 figures (last consulted on 12.10.19)

572

573 [2] International Olive Council (IOC). EU olive oil figures: production
574 Available on: http://www.internationaloliveoil.org/estaticos/view/131-world-olive-oil-
575 figures. (last consulted on 12.10.19).

576

577 [3] Dutournié P, Jeguirim M, Khiari B, Goddard M, Jellali S. Olive mill waste water:
578 From a pollutant to green fuels, agricultural water source, and bio-fertilizer. Part 2:
579 Water recovery. Water 2019;11(4):768.

580

581 [4] Cruz-Peragón F, Palomar JM, Ortega A. Integral energy cycle for the olive oil sector
582 in the province of Jaén. Grasas Aceites 2006;57:219-28.

583

584 [5] Annab H, Fiol N, Villaescusa I, Essamri A. A proposal for the sustainable treatment
585 and valorisation of olive mill wastes. J Environ Chem Eng 2019;7(1):102803.

586

587 [6] García-Maraver A, Zamorano M, Ramos-Ridao A, Díaz LF. Analysis of olive grove
588 residual biomass potential for electric and thermal energy generation in Andalusia
589 (Spain). Renewable and Sustainable Energy Reviews 2012;16:745-51.

590

591 [7] Christoforou E, Fokaides PA. A review of olive mill solid wastes to energy
592 utilization techniques. Waste Manage 2016;49:346-63.
593

594 [8] Tzathas K, Chrysagi E, Lyberatos G, Vlyssides A, Vlysidis A. Pretreatment of Olive
595 Mill Wastes for the Extraction of Residual Oil and High Added Value Compounds.
596 Waste Biomass Valoris 2019; DOI: 10.1007/s12649-019-00727-5
597

598 [9] Christoforou E, Kylili A, Fokaides PA. Technical and economical evaluation of
599 olive mills solid waste pellets. Renew Energy 2016;96:33-41.
600

601 [10] Khlifi S, Lajili M, Tabet F, Boushaki T, Sarh B. Investigation of the combustion
602 characteristics of briquettes prepared from olive mill solid waste blended with and
603 without a natural binder in a fixed bed reactor. Biomass Convers Biorefinery 2019;
604 DOI: 10.1007/s13399-019-00449-7
605

606 [11] Gómez-de la Cruz FJ, Casanova-Peláez PJ, Palomar-Carnicero JM, Cruz-Peragón
607 F. Drying kinetics of olive stone: a valuable source of biomass obtained in the olive oil
608 extraction. Energy 2014;75:146-52.
609

610 [12] Pattara C, Cappelletti GM, Cichelli A. Recovery and use of olive stones:
611 Commodity, environmental and economic assessment. Renewable and Sustainable
612 Energy Reviews 2010;14:1484-9.
613

614 [13] Gómez-De La Cruz FJ, Palomar-Carnicero JM, Casanova-Peláez PJ, Cruz-Peragón
615 F. Experimental determination of effective moisture diffusivity during the drying of
616 clean olive stone: Dependence of temperature, moisture content and sample thickness.
617 Fuel Process Technol 2015;137:320-6.
618
619 [14] Mata-Sánchez J, Pérez-Jiménez JA, Díaz-Villanueva MJ, Serrano A, Núñez-
620 Sánchez N, López-Giménez FJ. Development of olive stone quality system based on
621 biofuel energetic parameters study. Renewable Energy 2014;66:251-6.
622
623 [15] Mata-Sánchez J, Pérez-Jiménez JA, Díaz-Villanueva MJ, Serrano A, Núñez-
624 Sánchez N, López-Giménez FJ. Statistical evaluation of quality parameters of olive
625 stone to predict its heating value. Fuel 2013;113:750-6.
626
627 [16] Arjona R, Ollero P, Vidal FB. Automation of an olive waste industrial rotary dryer.
628 J Food Eng 2005;68:239-47.
629
630 [17] Castaño F, Rubio FR, Ortega MG. Modeling of a Cocurrent Rotary Dryer. Drying
631 Technol 2012;30:839-49.
632
633 [18] Fonseca-González N, Casanova-Kindelán J. Determination of the risk of fire in an
634 olive-oil mill waste dryer. Dyna 2016;91:694-701.
635
636 [19] Celma AR, Rojas S, López F, Montero I, Miranda T. Thin-layer drying behaviour
637 of sludge of olive oil extraction. J Food Eng 2007;80:1261-71.
638

639 [20] Montero I, Blanco J, Miranda T, Rojas S, Celma AR. Design, construction and
640 performance testing of a solar dryer for agroindustrial by-products. Energy Conversion
641 and Management 2010;51:1510-21.
642
643 [21] Montero I, Miranda T, Arranz JI, Rojas CV. Thin layer drying kinetics of by-
644 products from olive oil processing. International Journal of Molecular Sciences
645 2011;12:7885-97.
646
647 [22] Montero I, Miranda MT, Sepúlveda FJ, Arranz JI, Rojas CR, Nogales S. Solar
648 dryer application for olive oil mill wastes. Energies 2015;8:14049-63.
649
650 [23] Meziane S. Drying kinetics of olive pomace in a fluidized bed dryer. Energy
651 Conversion and Management 2011;52:1644-9.
652
653 [24] Liébanes MD, Aragón JM, Palancar MC, Arévalo G, Jiménez D. Fluidized bed
654 drying of 2-phase olive oil mill by-products. Drying Technol 2006;24:1609-18.
655
656 [25] Arjona R, García A, Ollero P. Drying of alpeorujo, a waste product of the olive oil
657 mill industry. J Food Eng 1999;41:229-34.
658
659 [26] Krokida MK, Maroulis ZB, Kremalis C. Process design of rotary dryers for olive
660 cake. Drying Technol 2002;20:771-88.
661

662 [27] Vega-Gálvez A, Miranda M, Díaz LP, Lopez L, Rodriguez K, Scala KD. Effective
663 moisture diffusivity determination and mathematical modelling of the drying curves of
664 the olive-waste cake. Bioresour Technol 2010;101:7265-70.
665
666 [28] Casanova-Peláez PJ, Palomar-Carnicero JM, Manzano-Agugliaro F, Cruz-Peragón
667 F. Olive cake improvement for bioenergy: the drying kinetics. Int J Green Energy
668 2015;12:559-69.
669
670 [29] Akgun NA, Doymaz I. Modelling of olive cake thin-layer drying process. J Food
671 Eng 2005;68:455-61.
672
673 [30] Doymaz I, Gorel O, Akgun NA. Drying characteristics of the solid by-product of
674 olive oil extraction. Biosystems Engineering 2004;88:213-9.
675
676 [31] Milczarek RR, Dai AA, Otoni CG, McHugh TH. Effect of shrinkage on isothermal
677 drying behavior of 2-phase olive mill waste. J Food Eng 2011;103:434-41.
678
679 [32] Gögüs F, Maskan M. Drying of olive pomace by a combined microwave-fan
680 assisted convection oven. Nahrung 2001;45:129-32.
681
682 [33] Ruiz Celma A, Rojas S, Lopez-Rodríguez F. Mathematical modelling of thin-layer
683 infrared drying of wet olive husk. Chemical Engineering and Processing: Process
684 Intensification 2008;47:1810-8.
685

686 [34] Gómez-de la Cruz FJ, Casanova-Peláez PJ, Palomar-Carnicero JM, Cruz-Peragón
687 F. Characterization and analysis of the drying real process in an industrial olive-oil mill
688 waste rotary dryer: A case of study in Andalusia. Appl Therm Eng 2017;116:1-10.
689
690 [35] Gómez-De La Cruz FJ, Casanova-Peláez PJ, Palomar-Carnicero JM, Cruz-Peragón
691 F. Modeling of olive-oil mill waste rotary dryers: Green energy recovery systems. Appl
692 Therm Eng 2015;80:362-73.
693
694 [36] Gómez-de la Cruz FJ, Casanova-Peláez PJ, Cruz-Peragón F, Palomar-Carnicero
695 JM. New Experimental Rotary Dryer of Olive Stone: Design, Control and Modeling.
696 Waste Biomass Valoris 2018;9:443-9.
697
698 [37] Vasić M, Grbavčić Ž, Radojević Z. Analysis of Moisture Transfer During the
699 Drying of Clay Tiles with Particular Reference to an Estimation of the Time-Dependent
700 Effective Diffusivity. Drying Technol 2014;32:829-40.
701
702 [38] Crank J. The mathematics of diffusion. Oxford, England: Clarendon Press, 1975.
703
704 [39] Gómez-de la Cruz FJ, Casanova-Peláez PJ, López-García R, Cruz-Peragón F.
705 Review of the Drying Kinetics of Olive Oil Mill Wastes: Biomass Recovery.
706 BioResources 2015;10:6055-80.
707
708 [40] Celma AR, Rojas S, López F, Montero I, Miranda T. Thin-layer drying behaviour
709 of sludge of olive oil extraction. J Food Eng 2007;80:1261-71.
710

711 [41] Gögüs F, Maskan M. Air drying characteristics of solid waste (pomace) of olive oil
712 processing. J Food Eng 2006;72:378-82.
713
714 [42] Freire F, Figueiredo A, Ferrão P. Modelling high temperature, thin layer, drying
715 kinetics of olive bagasse. J Agric Eng Res 2001;78:397-406.
716
717 [43] Batista LM, da Rosa CA, Pinto LA. Diffusive model with variable effective
718 diffusivity considering shrinkage in thin layer drying of chitosan. J Food Eng
719 2007;81:127-32.
720
721 [44] Sakin M, Kaymak-Ertekin F, Ilicali C. Modeling the moisture transfer during
722 baking of white cake. J Food Eng 2007;80:822-31.